Special Cases of DFT-Based Modulation and Demodulation for Affine Frequency Division Multiplexing

Vincent Savaux

Special Cases of DFT-Based Modulation and Demodulation for Affine Frequency Division Multiplexing

Vincent Savaux *Senior Member, IEEE*

***Abstract*—This paper deals with discrete Fourier transform (DFT)-based modulation and demodulation techniques for affine frequency division multiplexing (AFDM), as opposed to using the discrete affine Fourier transform (DAFT). This allows for a simple (de)modulation process based on the usual DFT, enabling the interpretation of AFDM as a precoded orthogonal frequency division multiplexing (OFDM) waveform. This makes the AFDM modulation scheme backward compatible with existing OFDM systems. Furthermore, the sampling frequency of the modulated AFDM signal can be finely tuned using the suggested methods, whereas the usual DAFT leads to signals sampled at the Nyquist rate. To achieve this, a DFT-based AFDM modulation technique is introduced, along with a corresponding demodulation method. The introduction considers necessary conditions on the AFDM signal parameters, albeit at the cost of reduced flexibility in parameter settings, as only a limited set of parameters can be considered. The validity of the presented method is supported by mathematical developments and proofs, and validated through simulations. Furthermore, a complexity analysis is conducted.**

***Index Terms*—AFDM, OCDM, OFDM.**

I. Introduction

New applications and use cases have emerged with the beyond-fifth generation of communications (5G) and the upcoming sixth generation (6G), accompanied by technical challenges that could not fully or optimally be overcome by means of the orthogonal frequency division multiplexing (OFDM) [1], [2]. Despite numerous advantages, such as the robustness against multipath channel or the cost-effective implementation through discrete Fourier transform (DFT) among others, new waveforms are being investigated to meet the ever-growing need for data rates. These waveforms should also allow for integrated holography, localization, sensing, and communication, while withstanding high time and frequency selectivity, as well as other radio impairments [2]–[5]. The most popular candidates are orthogonal time frequency space modulation (OTFS) [6], and chirp-based waveforms [7], such as orthogonal chirp division multiplexing (OCDM) [8], and affine frequency division multiplexing (AFDM) [9].

The OTFS is a block modulation that transforms the data symbols mapped on a 2-dimensional delay-Doppler domain into the time domain signal through an inverse symplectic Fourier transform, followed by a Heisenberg transform [6]. OTFS proves highly robust against doubly dispersive channels, given that the data is distributed across the delay-Doppler domain, and the block size can be adjusted accordingly. Moreover, OTFS supports multi-input multi-output (MIMO) [10], and slightly outperforms OFDM in radar and communications applications [11]. However, OTFS is complex, requiring 2-dimensional transforms and dedicated equalizers. Furthermore, due to its block modulation nature, it inevitably incurs larger latency than OFDM, dependent on the size of the spreading domain, and is not directly backward compatible with existing OFDM systems. These drawbacks may limit the adoption and deployment of OTFS in future communications systems.

The OCDM is similar to OFDM, but instead of using the DFT, it employs a discrete Fresnel transform (DFnT) [8]. Consequently, data symbols are transmitted via chirps rather than sinusoids, and any potential errors introduced by the doubly-selective channel are spread across the time-frequency grid. This spreading can be optimally decoded through an iterative process [12], [13], in contrast to OFDM, which is suboptimal against frequency-selective channels. Additionally, chirps possess an inherent property of good correlation, which is relevant for radar, sensing, and communication purposes [14]. In a study [15], the authors show that OCDM can be used in multi-user MIMO systems, by applying precoding (typically zero forcing) in time domain or in chirp domain (Fresnel domain). Interestingly, the authors of [16], [17] demonstrated that the OCDM signal can be generated through a simple IDFT preceded by a precoding stage, which includes a DFT and a multiplication by a chirp. The resulting signal can be modulated at any sampling rate, as guard bands can be added prior to the IDFT, whereas the IDFnT leads to signals sampled at Nyquist rate [8]. Consequently, the OCDM can be interpreted as a chirp-precoded OFDM waveform, similar to DFT-spread-OFDM, and is therefore straightforwardly backward compliant with existing standards. However, the performance of OCDM may degrade in the case of high mobility [4].

The AFDM, originally described in [9], is based on the discrete affine Fourier transform (DAFT) [18]–[20]. It is noteworthy that continuous affine Fourier transform (AFT) modulation was used ten years prior to [9] in [21], [22]. Essentially, AFDM can be interpreted as a generalization of OCDM, allowing for the transmission of more than one chirp (not necessarily integer) within a symbol duration. Consequently, AFDM effectively spreads errors better than OCDM, making it more robust to Doppler spread [4], [9], [23]. Few papers dealing with AFDM have been published to date, and numerous challenges are still pending. For instance, [24] shows that the AFDM outperforms the OFDM to sense targets and achieves performance comparable with OTFS [25], [26] investigates the performance of MIMO-AFDM in doubly-selective channels, and [9], [27]–[30] address pilot design, channel estimation, and equalization for the AFDM modulation scheme. However, it is worth noting that all these papers consider AFDM signals obtained through IDAFT and then sampled at Nyquist rate, which imposes limitations on numerous applications.

In this paper, we introduce DFT-based modulation and demodulation methods for AFDM, enabling the generation of

Manuscript submitted 2023

Vincent Savaux is with Institute of Research and Technology b<>com, Rennes, France (e-mail: vincent.savaux@b-com.com, Phone: +33 256 35 82 16.)

signals at any sampling rate using the usual IDFT. Similar to [16], [17] in OCDM, we demonstrate that the AFDM modulation can be interpreted as a chirp-precoded OFDM. This modulation technique offers various advantages. In the frequency domains, guard bands can be directly added (during the modulation process) at the edges of the spectrum or between adjacent signals in mixed-numerology use case. Simple frequency equalization can be performed, limiting the complexity of the AFDM receiver. MIMO precoder can be inserted in the frequency domain to mitigate the interference inter-user, similar to what is commonly done in OFDM. More generally, the DFT-based AFDM (de)modulation is straightforwardly backward compatible with OFDM systems, potentially facilitating the adoption of AFDM for future deployments. The contributions of this paper are summarized as follows:

- The derivation of the DFT-based AFDM is mathematically proven, subject to specific necessary conditions. Notably, we demonstrate that the number of chirps per symbol should be limited to an integer value (where one chirp corresponds to OCDM). Additionally, the ratio between the number of subcarriers and the number of chirps per symbol should be an integer as well.
- The DFT-based AFDM modulation can be interpreted as a precoding stage comprising a DFT and multiplication by a chirp, followed by an IDFT of any desired size (similar to pre-coded OFDM).
- The complexity of the proposed technique is compared with a benchmark solution, which involves a standard AFDM modulation followed by a DFT/IDFT upsampling stage. It is demonstrated that the proposed solution requires only two (I)DFT operations instead of three, and the sparsity of the DFT allows for complexity reduction. This makes the proposed DFT-based AFDM modulation scheme less complex than the benchmark solution.
- The relevance of the suggested approach is illustrated by simulation results, confirming the common observation that AFDM outperforms OFDM in terms of Bit Error Rate (BER) under various sources of distortion, including filtering, interference, and channel effects. Additionally, it is shown that the performance of AFDM is comparable to that of OTFS.

The rest of the paper is organized as follows: Section II introduces the AFDM waveform, and Section III presents the suggested DFT-based AFDM modulation method and the complexity analysis. In Section IV, the corresponding DFT-based AFDM demodulation is described. Numerical results are presented in Section V and Section VI concludes this paper.

Notations: Boldface **a** is used for vectors and matrices, while normal font a indicates scalar variables. The Kronecker product on matrices is denoted by $(.\otimes.)$. $\mathbb{1}_\Omega$ is the indicator function of the elements belonging to the set Ω. Moreover, $2\mathbb{Z}$ and $\mathbb{Z}\backslash 2\mathbb{Z}$ are the subsets of $\mathbb{Z}$ corresponding to even and odd integers, respectively.

II. AFDM System Model

As mentioned earlier, the AFDM signal is based on DAFT, originally described in [18], popularized in [20], and updated in [9], [27]. For this reason, we use similar notations as in [9], [27] to introduce the AFDM waveform. Essentially, it is a multicarrier signal where the data symbols are carried by chirps. Thus, the AFDM signal x_n, $n=0,1,..,N-1$, when sampled at Nyquist rate, can be expressed as

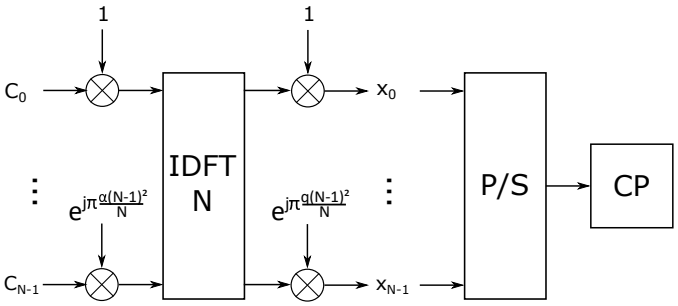

Fig. 1. Basic AFDM modulation based on a multiplication of the data symbols C_m by $e^{\frac{j\pi\alpha m^2}{N}}$, an IDFT of size N, and a multiplication of the resulting samples by $e^{\frac{j\pi qn^2}{N}}$.

$$x_n = \frac{1}{\sqrt{N}} \sum_{m=0}^{N-1} C_m \underbrace{\exp\Big(\frac{j\pi}{N}(qn^2+\alpha m^2+2mn)\Big)}_{\phi_{m,n}}, \quad (1)$$

where m is the chirp index, N is the number of carrier chirps (also the number of samples per symbol) and $(q,\alpha)\in\mathbb{R}$ are two chirp parameters that will be set afterward. It is worth noticing that $q=\alpha=-1$ leads to the OCDM [8], and $q=\alpha=0$ leads to the OFDM. Furthermore, we introduce the function $\phi_{m,n}$ (also called the pulse shape) for the sake of clarity in the following developments. By rewriting (1) as

$$x_n = \frac{e^{\frac{j\pi qn^2}{N}}}{\sqrt{N}} \sum_{m=0}^{N-1} C_m e^{\frac{j\pi\alpha m^2}{N}} e^{\frac{2j\pi mn}{N}}, \quad (2)$$

we notice that the AFDM modulation consists in a multiplication of the data symbols C_m by $e^{\frac{j\pi\alpha m^2}{N}}$, then an IDFT of size N, and a multiplication of the resulting samples by $e^{\frac{j\pi qn^2}{N}}$, such as illustrated in Fig. 1. Such as indicated in [20], the functions $\phi_{m,n}$, $n=0,1,..,N-1$, form an orthonormal basis for the space of chirp-periodic signals. Furthermore, such as indicated in [9], a so-called *chirp-periodic* prefix (CPP) can be added in order to cope with multipath channel. If we denote by N_{CP} the CPP length, then the periodicity of the chirps holds if, for any $n=-N_{CP},..,1$, we have

$$x_n = x_{N+n} e^{-2j\pi \frac{q}{N}(N^2+2Nn)}, \quad (3)$$

which reduces to a usual cyclic prefix (CP) if q is an integer. Since we assume that the latter assumption holds throughout the paper, then we consider a simple CP such as indicated in Fig. 1.

It is worth emphasizing that, despite its simplicity of implementation, the AFDM modulation described in (2) and Fig. 1 suffers from two main drawbacks: firstly it only generates signals sampled at Nyquist rate, whereas it is desirable to obtain a tunable sampling rate to feed the digital to analog converter (DAC) in practical applications. As it is, an oversampling process based on polynomial or DFT/IDFT interpolation is mandatory, as illustrated in Fig. 2-(a) and referred as benchmark solution in the following. In this case, three (I)DFT must be implemented in the AFDM modulation. On the other hand, the schemes in Figs. 1 and 2-(a) are not directly backward compatible with other multicarrier modulations such as OCDM, OFDM, or precoded OFDM, which may limit the deployment of AFDM. For this reasons, in the following we suggest an original technique of AFDM modulation based on a precoding step followed by an IDFT whose size is tunable leading to desirable

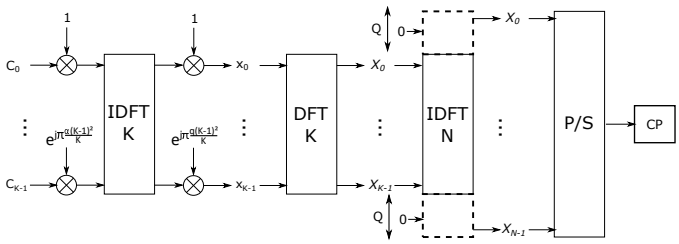

(a) AFDM modulation, benchmark solution.

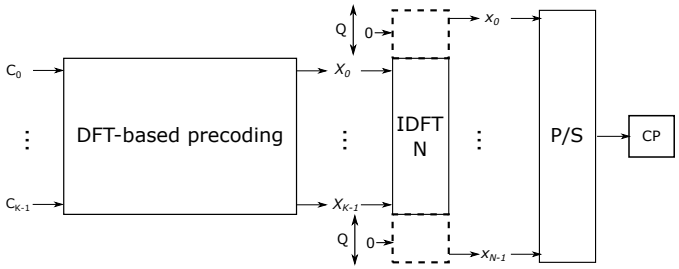

(b) AFDM modulation as DFT-precoded OFDM.

Fig. 2. AFDM modulation: benchmark solution (a) based on IDFT/DFT/IDFT and chirp multiplication; proposed solution (b) based on a precoding step followed by an IDFT.

sampling rate, which can be generally illustrated as in Fig. 2-(b), along with alternative implementations of the same method.

III. DFT-Based AFDM Modulation

In this section, we present a solution for an AFDM modulation scheme based on a precoding step followed by an IDFT, by rewriting (1)-(2) under conditions on q and N. To this end, several steps are mandatory to achieve the expected goal. First, we introduce the q-DFT of size N, which means that:

- q-DFT is a DFT if $q<0$, and the DFT matrix coefficients are $\frac{e^{-2j\pi\frac{mn}{N}}}{\sqrt{N}}$ for $m,n=0,1,..,N-1$,
- q-DFT is an IDFT if $q>0$, and the IDFT matrix coefficients are $\frac{e^{2j\pi\frac{mn}{N}}}{\sqrt{N}}$.

The basic principle of the following method lies in expressing $\phi_{m,n}$ as an IDFT of another function, which can in turn be interpreted as a precoding stage. This principle has been used in [16], [17] to expressed the OCDM modulation based on IDFT, and is hereby generalized to AFDM.

A. General Solution

First, it must be noticed that if q is an integer, and if q or N is even, we can rewrite the DFT of $\phi_{m,n}$, denoted by $\Phi_{m,k}$, with $m,n,k=0,1,..,N-1$, by using the generalized quadratic Gauss sum [31] (see Theorem 1.2.4):

$$\begin{aligned}\Phi_{m,k}&=\frac{1}{\sqrt{N}}\sum_{n=0}^{N-1}\phi_{m,n}e^{-2j\pi\frac{kn}{N}}\\&=\frac{e^{\frac{j\pi\alpha m^2}{N}}}{\sqrt{N}}\sum_{n=0}^{N-1}\exp\Big(\frac{j\pi}{N}(qn^2+2(m-k)n)\Big)\\&=\frac{1}{\sqrt{|q|}}\underbrace{e^{j\frac{\varepsilon_q\pi}{4}}\exp\Big(\frac{j\pi m^2\big(\alpha-\frac{1}{q}\big)}{N}\Big)}_{A_m/\sqrt{|q|}}\\&\quad\times\exp\Big(\frac{j\pi}{qN}(-k^2+2mk)\Big)\\&\quad\times\underbrace{\sum_{r=0}^{|q|-1}\exp\Big(\frac{-j\pi}{q}(Nr^2+2(m-k)r)\Big)}_{B_{m,k,q}},\end{aligned}\tag{4}$$

where $\varepsilon_q=\text{sign}(q)$. We introduce the notation A_m and $B_{m,k,q}$ in (4) for clarity matter. A general solution is then given by substituting the IDFT of $\Phi_{m,k}$ into (1) as:

$$\begin{aligned}x_n&=\frac{1}{\sqrt{N}}\sum_{m=0}^{N-1}C_m\times\frac{1}{\sqrt{N}}\sum_{k=0}^{N-1}\Phi_{m,k}e^{2j\pi\frac{kn}{N}}\\&=\frac{1}{|q|N}\sum_{m=0}^{N-1}C_mA_m\sum_{k=0}^{N-1}B_{m,k,q}\\&\quad\times\exp\Big(\frac{j\pi}{qN}(-k^2+2mk)\Big)e^{2j\pi\frac{kn}{N}}\\&=\frac{1}{\sqrt{N}}\sum_{k=0}^{N-1}e^{-j\pi\frac{k^2}{qN}}\sum_{r=0}^{|q|-1}\exp\Big(\frac{-j\pi}{q}(Nr^2-2kr)\Big)\\&\quad\times\underbrace{\frac{1}{|q|\sqrt{N}}\sum_{m=0}^{N-1}C_mA_me^{-2j\pi\frac{mr}{q}}e^{2j\pi\frac{km}{qN}}e^{2j\pi\frac{kn}{N}}}_{G_{k,r}}\\&=\sum_{r=0}^{|q|-1}e^{-j\pi\frac{Nr^2}{q}}\underbrace{\frac{1}{\sqrt{N}}\sum_{k=0}^{N-1}e^{-j\pi\frac{k^2}{qN}}e^{2j\pi\frac{kr}{q}}G_{k,r}e^{2j\pi\frac{kn}{N}}}_{H_{n,r}},\end{aligned}\tag{5}$$

where we recognize that $G_{k,r}$ is the q-DFT of size $|q|N$ of $C_mA_me^{-2j\pi\frac{mr}{q}}$, and $H_{n,r}$ is the IDFT of $e^{-j\pi\frac{k^2}{qN}}e^{2j\pi\frac{kr}{q}}G_{k,r}$. Alternatively, by inverting both sums, we obtain:

$$x_n=\frac{1}{\sqrt{N}}\sum_{k=0}^{N-1}\Big[\sum_{r=0}^{|q|-1}e^{-j\pi\frac{Nr^2}{q}}e^{-j\pi\frac{k^2}{qN}}e^{2j\pi\frac{kr}{q}}G_{k,r}\Big]e^{2j\pi\frac{kn}{N}}.\tag{6}$$

It is worth mentioning that this general solution may be too complex for practical implementation as it requires $|q|$ q-DFT of size $|q|N$ and one IDFT of size N. However, it is a first mandatory step (obtaining (4) especially) introducing the suggested DFT-based solution such as presented afterward.

B. Suggested Solution

1) Preliminaries: It has been stated that the previous general solution is too complex in practice. The main reason is the presence of the sum leading to $B_{m,k,q}$ in (4). Besides complexity, the general solution still leads to a signal x_n sampled at Nyquist rate. As a consequence, the suggested approach is to find conditions allowing for the simplification of $B_{m,k,q}$. Thus, it can be noticed

that if $\frac{N}{q}$ is even (in that case N must be even, and q can be even or odd), or if $\frac{N}{q}$ is odd (in that case both N and q are even), $B_{m,k,q}$ can be simplified. In both cases, it must be noticed that the aforementioned conditions to apply the generalized quadratic Gauss sum [31] hold. In the case where $\frac{N}{q}$ is even, we obtain:

$$\begin{aligned} B_{m,k,q} &= \sum_{r=0}^{|q|-1} \exp\Big(\frac{-2j\pi r}{q}(m-k)\Big) \\ &= \begin{cases} 0, & \text{if } (m-k)\text{mod } q \neq 0 \\ |q|, & \text{else} \end{cases} \\ &= |q|\mathbb{1}_{(m-k)\text{mod } q=0}. \end{aligned} \tag{7}$$

Otherwise, in the case where $\frac{N}{q}$ is odd, we obtain:

$$\begin{aligned} B_{m,k,q} &= \sum_{r=0}^{|q|-1} (-1)^r \exp\Big(\frac{-2j\pi r}{q}(m-k)\Big) \\ &= \begin{cases} |q|, & \text{if } \frac{2(m-k)}{q} \text{ is odd} \\ 0, & \text{else} \end{cases} \\ &= |q|\mathbb{1}_{\frac{2(m-k)}{q} \in \mathbb{Z}\setminus 2\mathbb{Z}}. \end{aligned} \tag{8}$$

To limit the length of the paper, we focus on the developments and proofs regarding the case where $\frac{N}{q}$ is even (7). However, it is noteworthy that the case where $\frac{N}{q}$ is odd (8) can be straightforwardly addressed using the same developments. The main results for this case will also be provided (without additional proof).

By assuming that $\frac{N}{q}$ is even, we can express $\Phi_{m,k}$ from (4) and (7) as

$$\begin{aligned} \Phi_{m,k} = \mathbb{1}_{(m-k)\text{mod } q=0} \underbrace{\sqrt{|q|} e^{j\frac{\varepsilon_q \pi}{4}} \exp\Big(\frac{j\pi m^2 \big(\alpha - \frac{1}{q}\big)}{N}\Big)}_{A_m} \\ \times \exp\Big(\frac{j\pi}{qN}(-k^2+2mk)\Big), \end{aligned} \tag{9}$$

where we recognize A_m such as previously defined. We show in Appendix A that we actually found $\phi_{m,n}$ by applying the IDFT to $\Phi_{m,k}$, *i.e.* $\phi_{m,n} = \frac{1}{\sqrt{N}} \sum_{k=0}^{N-1} \Phi_{m,k} e^{2j\pi \frac{kn}{N}}$, which proves the validity of (9). Thus, (1) can be rewritten as

$$\begin{aligned} x_n &= \sum_{m=0}^{N-1} C_m \times \frac{1}{\sqrt{N}} \sum_{k=0}^{N-1} \Phi_{m,k} e^{2j\pi \frac{kn}{N}} \\ &= \frac{1}{\sqrt{N}} \sum_{k=0}^{N-1} \Big[\sum_{m=0}^{N-1} C_m A_m \mathbb{1}_{(m-k)\text{mod } q=0} \\ &\quad \times \exp\Big(\frac{j\pi}{qN}(-k^2+2mk)\Big)\Big] e^{2j\pi \frac{kn}{N}} \\ &= \frac{1}{\sqrt{N}} \sum_{k=0}^{N-1} e^{-j\pi \frac{k^2}{qN}} \Big[\sum_{m=0}^{N-1} C_m A_m \mathbb{1}_{(m-k)\text{mod } q=0} e^{2j\pi \frac{mk}{qN}} \Big] \\ &\quad \times e^{2j\pi \frac{kn}{N}}. \end{aligned} \tag{10}$$

We can generalize (10) to consider a DFT of size $K \leq N$ corresponding to K symbols of data $\{C_0, C_1, .., C_{K-1}\}$ and a IDFT of size N. In that case $Q = \frac{N-K}{2}$ null subcarriers are located at the edge of the band such as illustrated in Fig. 2. Therefore, x_n becomes:

$$\begin{aligned} x_n = \frac{1}{\sqrt{N}} \sum_{k=0}^{N-1} \beta_k e^{-j\pi \frac{(k-Q)^2}{qK}} \\ \times \Big[\sum_{m=0}^{K-1} C_m A_m \mathbb{1}_{(m-(k-Q))\text{mod } q=0} e^{2j\pi \frac{m(k-Q)}{qK}} \Big] e^{2j\pi \frac{kn}{N}}, \end{aligned} \tag{11}$$

where the oversampling rate $\frac{N}{K}$ can be finely tuned. Furthermore $\beta_k = 1$ if $Q \leq k \leq N-Q-1$, and $\beta_k = 0$ else, highlighting the null subcarriers at the edges of the band.

It is also possible to rewrite (11) from scalar to a matrix form such as:

$$\mathbf{x} = \boldsymbol{\mathcal{F}}_N^H \mathbf{O} \mathbf{D}_c \mathbf{T} \sum_{r=0}^{|q|-1} \mathbf{I}_r \boldsymbol{\mathcal{F}}_{|q|K}^{(q)} \mathbf{A}_r \mathbf{c}_r, \tag{12}$$

where

$$\mathbf{c}_r = [0,..,C_r,0,..,C_{r+|q|},..,C_{r+K-|q|}, \overbrace{0, \quad .. \quad ,0}^{(|q|-1)K-r+|q|-1}]^T$$

is a $|q|K \times 1$ vector containing part of the constellation symbols ($\frac{K}{|q|}$ among K) at indexes $\{r, r+|q|, .., r+K-|q|\}$, with $r = |m \ mod \ q| = m \ mod \ |q| \in \{0,1,..,|q|-1\}$ and zero otherwise. The matrix $\mathbf{A}_r$ is a $|q|K \times |q|K$ diagonal matrix containing the vector $[0,..,A_r,0,..,A_{r+|q|},..,A_{r+K-|q|}, \overbrace{0, \quad .. \quad ,0}^{(|q|-1)K-r+|q|-1}]$ on its diagonal, *i.e.* indexes of C_r and A_r match. $\mathbf{I}_r$ is also a $|q|K \times |q|K$ diagonal matrix containing the vector $[0,..,1,0,..,1,..,1,0,..,0]$ on its diagonal, where the entries 1 are located at indexes $\{r, r+|q|, .., r+|q|(K-1)\}$. This vector highlights the indicator function $\mathbb{1}_{(m-k)mod\ q=0}$ in (11). $\mathbf{T} = [\mathbf{Id}_K, \mathbf{0}_{K\times(q-1)K}]$ is a $K \times qK$ matrix where $\mathbf{Id}_K$ is the $K \times K$ identity matrix, and $\mathbf{0}_{K\times(q-1)K}$ is the $K \times (q-1)K$ zero matrix. $\mathbf{D}_c$ is the $K \times K$ diagonal matrix containing the elements $e^{-j\pi \frac{k^2}{qK}}$, $k = 0,1,..,K-1$ on its diagonal. The $N \times K$ matrix $\mathbf{O} = [\mathbf{0}_{Q\times K}; \mathbf{Id}_K; \mathbf{0}_{Q\times K}]$ corresponds to the null carrier concatenation at the edge of the band. We also denote by $\boldsymbol{\mathcal{F}}_N$ and $\boldsymbol{\mathcal{F}}_N^H$ the DFT and IDFT matrices of size $N \times N$, and $\boldsymbol{\mathcal{F}}_{|q|K}^{(q)}$ the q-DFT matrix of size $|q|K \times |q|K$.

In the case where $\frac{N}{q}$ is odd, the expression of x_n is similar, except that $\mathbb{1}_{(m-k)mod\ q=0}$ is substituted by $\mathbb{1}_{\frac{2(m-k)}{q} \in \mathbb{Z}\setminus 2\mathbb{Z}}$ in (9)-(11). The matrix form (12), in turn, remains similar except that $\mathbf{I}_r$ is substituted by $\mathbf{I}_{r+\frac{|q|}{2}}$, where $\mathbf{I}_{r+\frac{|q|}{2}}$ is a $|q|K \times |q|K$ diagonal matrix containing the vector $[0,..,1,0,..,1,..,1,0,..,0]$ on its diagonal, where the entries 1 are located at indexes $\{r+\frac{|q|}{2}, r+|q|+\frac{|q|}{2}, .., (r+|q|(K-1)+\frac{|q|}{2}) \text{mod} |q|K\}$. Note that in the rest of the paper, we assume that $\frac{N}{q}$ is an integer (even or odd).

Remark 1. *It is worth emphasizing that the fact that q and $\frac{N}{q}$ are integers is not a limiting feature to achieve full-diversity, although in [9], it is more generic as q can take any real value. In fact, according to [9], the parameters q should satisfy $q > \alpha_{max}$ where α_{max} stands for the maximum Doppler shift normalized by the subcarrier spacing. Since q is real-valued in [9], the exact equality condition $q = \alpha_{max} + \frac{1}{2}$ can be achieved, but i) it assumes a perfect knowledge of α_{max}, which is a strong assumption in practice, ii) in this paper, the inequality condition $q > \alpha_{max}$ with q integer guarantees full-diversity, while relaxing the assumption on the perfect knowledge of α_{max}. To satisfy $q > \alpha_{max}$ with q integer, it is sufficient to set $q = \lceil \alpha_{max} \rceil$.*

2) AFDM as Precoded OFDM: The suggested solution in Proposition 1 aims at expressing the AFDM modulation as a precoded OFDM while removing the sums involved in the previous solution (12) formulated in preliminaries. The corresponding AFDM modulation is illustrated in Fig. 3.

Proposition 1. *The AFDM modulated signal can be expressed as*

$$\boldsymbol{x} = \boldsymbol{\mathcal{F}}_N^H \boldsymbol{O} \boldsymbol{D}_c \boldsymbol{T} \boldsymbol{\mathcal{F}}_{|q|K}^{(q)} \boldsymbol{\gamma}, \tag{13}$$

where $\boldsymbol{\gamma}$ is a vector of size $|q|K \times 1$ defined as

$$\boldsymbol{\gamma} = \boldsymbol{D}_J \boldsymbol{Ac}, \tag{14}$$

with $\boldsymbol{Ac}$ a $|q|K \times 1$ vector defined as

$$\boldsymbol{Ac} = [\overbrace{1,..,1}^{|q|}]^T \otimes [A_0 C_0,..,A_{K-1} C_{K-1}]^T,$$

and $\boldsymbol{D}_J$ is the diagonal matrix of size $|q|K \times |q|K$, whose diagonal vector is given by

$$\boldsymbol{V}_J = [\boldsymbol{V}_{J,0},..,\boldsymbol{V}_{J,r},..,\boldsymbol{V}_{J,|q|-1}],$$

and each vector $\boldsymbol{V}_{J,r}$ is of size $1 \times K$ and contains, for $r = 0,1,..,|q|-1$ and $m = 0,1,..,K-1$ (and assuming $\frac{N}{|q|}$ even):

$$V_{J,r,m} = \frac{1}{|q|} \exp\Big(-\frac{2j\pi r}{q}(m \ mod |q|)\Big). \tag{15}$$

In the case where $\frac{N}{|q|}$ is odd, then $V_{J,r,m}$ in (15) should be substituted by

$$V_{J,r,m+\frac{|q|}{2}} = \frac{1}{|q|} \exp\Big(-\frac{2j\pi r}{q}((m+\frac{|q|}{2}) \ mod |q|)\Big). \tag{16}$$

Proof. First, we can rewrite (12) by putting the q-DFT of size $|q|K$ outside the sums in order to compute it only once. To this end, we define the $|q|K \times |q|K$ matrix $\mathbf{J}_r = (\boldsymbol{\mathcal{F}}_{|q|K}^{(q)})^H \mathbf{I}_r \boldsymbol{\mathcal{F}}_{|q|K}^{(q)}$, then (12) can be rewritten as

$$\mathbf{x} = \boldsymbol{\mathcal{F}}_N^H \mathbf{O} \mathbf{D}_c \mathbf{T} \boldsymbol{\mathcal{F}}_{|q|K}^{(q)} \sum_{r=0}^{|q|-1} \mathbf{J}_r \mathbf{A}_r \mathbf{c}_r, \tag{17}$$

It can be straightforwardly shown that, for any $r = 0,1,..,|q|-1$, $u,v = 0,1,..,|q|K-1$, the (u,v)-th entry of $\mathbf{J}_r$ (assuming $\frac{N}{|q|}$ even) is given by

$$\mathbf{J}_r(u,v) = \begin{cases} 0, & \text{if } (u-v) \bmod K \neq 0 \\ \frac{1}{|q|} \exp\Big(2j\pi r \frac{v-u}{qK}\Big), & \text{else} \end{cases}. \tag{18}$$

In the case where $\frac{N}{|q|}$ is odd, r is substituted by $(r+\frac{|q|}{2}) \bmod |q|$ such that we obtain

$$\mathbf{J}_{(r+\frac{|q|}{2}) \bmod |q|}(u,v) = \begin{cases} 0, & \\ \text{if } (u-v) \bmod K \neq 0 & \\ \frac{1}{|q|} \exp\Big(2j\pi((r+\frac{|q|}{2}) \bmod |q|) \frac{v-u}{qK}\Big), & \\ \text{else} & \end{cases}. \tag{19}$$

Then, by noticing that $\mathbf{D}_J \mathbf{Ac} = \sum_{r=0}^{|q|-1} \mathbf{J}_r \mathbf{A}_r \mathbf{c}_r$, (17) directly leads to (13), which concludes the proof. □

It can be observed that, unlike (12), (13) does not involve the sum of signal components from different branches, as it is substituted by a copy of the vector $[A_0 C_0,..,A_{K-1} C_{K-1}]^T$. Furthermore, the proposed DFT-based AFDM modulation (13) involves one q-DFT of size $|q|K$ and one IDFT of size N. Fig. 3 highlights the expected structure of precoded OFDM consisting in a precoding step composed of the multiplication of the constellation elements by $\mathbf{D}_J \mathbf{A}$, the copies, the q-DFT, and the multiplication by $\mathbf{D}_c$. It is followed by the IDFT of size N such as shown in Fig. 2-b. Most important, a corresponding demodulation process can be deduced from (13) thanks to the use of the copies. Prior to the DFT-based AFDM demodulation, a complexity comparison between the benchmark solution Fig. 2-(a) and the suggested one in Fig. 2-(b) using (13) is carried out.

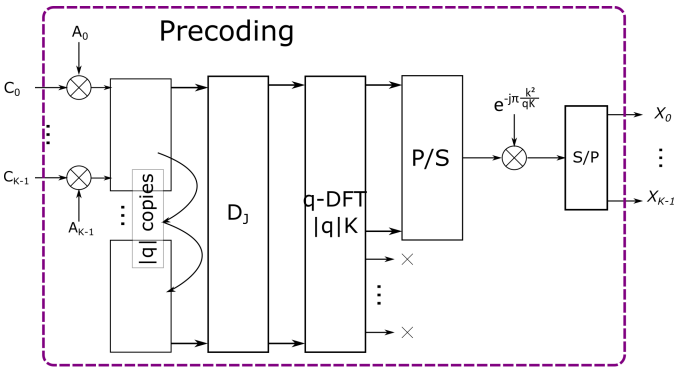

Fig. 3. Focus on the precoding of the DFT-based AFDM modulation, which can be seen as a precoded OFDM.

C. Complexity Analysis

In this section, we analyze the complexity of the suggested DFT-based AFDM modulation (13), which is similar to a precoded OFDM, in comparison with the benchmark solution described in Fig. 2-(a). The latter is based on the usual AFDM modulation (2) followed by a DFT/IDFT upsampling stage. The complexity is assessed in terms of the number of complex multiplications, with additions omitted. For the sake of simplicity, the (I)DFTs are assumed to involve $N\log(N)$ multiplications, where N is the DFT size.

a) Benchmark Solution: According to Fig. 2-(a), the benchmark solution for AFDM modulation consists of two phase multiplications ($e^{\frac{j\pi q n^2}{K}}$ and $e^{\frac{j\pi \alpha m^2}{K}}$, with $n,m = 0,1,..,K-1$), two (I)DFT of size K, and one IDFT of size N. The overall complexity of the benchmark solution is then

$$2K + 2K\log(K) + N\log(N).$$

b) Suggested Solution: We first assess the complexity of the suggested DFT-based AFDM in Fig. 3 directly from (13), and then we suggest further complexity reductions for (13). Thus, (13) naively consists of three phase multiplications (namely $\mathbf{Ac}$ of size K, $\mathbf{D}_J$ of size $|q|K$, and $\mathbf{D}_c$ of size K), one q-DFT of size $|q|K$, and one IDFT of size N. The overall complexity of "naive" (13) is then $(2+|q|)K + |q|K\log(|q|K) + N\log(N)$. We could then deduce that the suggested solution is more cost-effective than the benchmark solution only if $|q| = 1$ (corresponding to OCDM), which has been already shown in [16], [17]. For larger values of $|q|$, it would be advantageous to consider the benchmark solution. However, it can be noticed in (18) that for values of $|q| \in \{1,2,4\}$, the multiplication by $\mathbf{D}_J$ only yields changes of sign ± 1 or $\pm j$, which reduces the number of multiplications to zero. Furthermore, it is well-known that the complexity of a (I)DFT (of size N) with sparse input (of size $K \leq N$) can reduced to $K\log(N)$. Interestingly, it has been recently shown in [32] that such a reduction of complexity can be achieved for (I)DFT with sparse output as well. Since K samples among the $|q|K$ samples of the q-DFT are kept in the proposed AFDM modulation method (see Fig. 3), then the algorithm from [32] can be used to reduce

TABLE I
COMPLEXITY COMPARISON OF AFDM MODULATION METHODS BASED ON THE BENCHMARK SOLUTION (FIG. 2-(A)), AND THE PROPOSED SOLUTION (13). FOR THE LATTER (A) INDICATES THAT $|q| \notin \{1,2,4\}$ AND (B) THAT $|q| \in \{1,2,4\}$.

Solution	Complexity
Benchmark	$2K+2K\log(K)+N\log(N)$
Proposed (a)	$(2+\|q\|)K+K\log(\|q\|K)+N\log(N)$
Proposed (b)	$2K+K\log(\|q\|K)+N\log(N)$

the complexity of the DFT-precoding to $K\log(|q|K)$. Therefore, the overall complexity of the proposed algorithm can be upper bounded (independently of the value of q) by

$$(2+|q|)K+K\log(|q|K)+N\log(N)$$

and in the case where $|q| \in \{1,2,4\}$ then $(2+|q|)K$ even reduces to $2K$.

The complexity analysis is summarized in Table I where (a) and (b) indicate that $|q| \notin \{1,2,4\}$ and $|q| \in \{1,2,4\}$, respectively. It is worth emphasizing that if the last IDFT of size N is omitted (since it is common to all solutions), then the complexity of the proposed solution ((a) and (b)) is asymptotically half that of the benchmark solution, for large K values. For lower K values, it can be noticed that (a) is less complex that the benchmark solution if the following relation holds:

$$2K+2K\log(K) \geq (2+|q|)K+K\log(|q|K)$$
$$\Leftrightarrow \qquad \log\left(\frac{K}{|q|}\right) \geq |q|.$$

To further illustrate the complexity of the AFDM modulation techniques, Fig. 4 shows the overall complexity of the techniques (log scale) listed in Table I versus $\log_2(K)$ for $K \in [[16,4096]]$, and considering $N=2K$ and $q=-4$. It is noteworthy that the proposed solution (a) has been plotted even if $q=-4$ (whereas it could allow us to only consider the complexity (b)), but it illustrates the behavior of (a) compared to the benchmark solution. First, it can be observed that the suggested solution (b) is less complex than the benchmark for any considered K value, while solution (a) is less complex that the benchmark solution (resp. more complex) for $K \geq 64$ (resp. for $K \leq 64$). Moreover, the fact that the complexity of all solutions seems to be close to each other is due to the fact that $N=2K$ and is then mainly due to the last IDFT of size N. In any case, we conclude that the proposed DFT-based AFDM modulation is less computationally expensive to implement than the benchmark solution, while guaranteeing backward compatibility with OFDM systems.

IV. AFDM RECEPTION

A. DFT-Based AFDM Receiver

This section is dedicated to the presentation of a DFT-based AFDM receiver based on the previous AFDM modulation. To this end, we first introduce Proposition 2, which shows the relationship between the elements of the output of the q-DFT $\boldsymbol{\mathcal{F}}^{(q)}_{|q|K}\boldsymbol{\gamma}$ (from (13)), allowing to recover the whole $|q|K \times 1$ data vector from the truncated one $\mathbf{T}\boldsymbol{\mathcal{F}}^{(q)}_{|q|K}\boldsymbol{\gamma}$ of size $K \times 1$.

Proposition 2. *If we note $\mathbf{W}=\boldsymbol{\mathcal{F}}^{(q)}_{|q|K}\boldsymbol{\gamma}$ from (13) the $|q|K \times 1$ vector of the output of the q-DFT, then for any $k=0,1,..,K-1$, and $p=0,..,|q|-1$, the elements W_{k+pK} of $\mathbf{W}$ follow the property (assuming $\frac{N}{|q|}$ is even):*

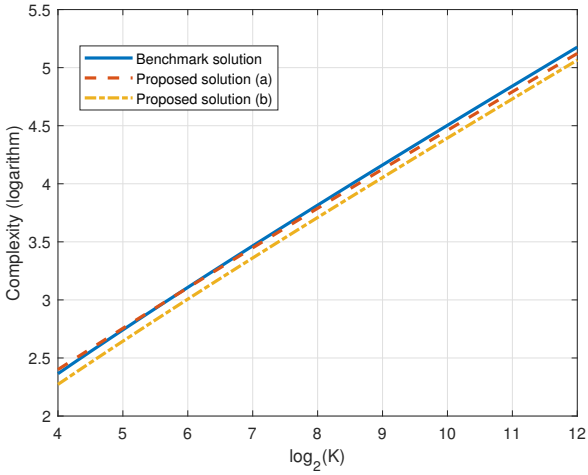

Fig. 4. Complexity comparison of AFDM modulations methods (log scale) versus $\log_2(K)$: benchmark solution and proposed solution, considering $N=2K$ and $q=-4$.

$$W_{k+pK} = W_k e^{2j\pi\frac{kp}{q}}. \tag{20}$$

In the case where $\frac{N}{|q|}$ is odd, then the following equality holds:

$$W_{k+pK} = (-1)^p W_k e^{2j\pi\frac{kp}{q}}. \tag{21}$$

Proof. The proof is carried out for $\frac{N}{|q|}$ even. For any $k=0,1,..,|q|K-1$, and $s=0,1,..,|q|K-1$, the elements W_k of $\mathbf{W}$ can be expressed as

$$\begin{aligned} W_k &= (\boldsymbol{\mathcal{F}}^{(q)}_{|q|K}\boldsymbol{\gamma})(k) \\ &= \sum_{s=0}^{|q|K-1} (Ac)_s V_{J,s} \exp\Big(\frac{2j\pi ks}{qK}\Big), \end{aligned} \tag{22}$$

where $(Ac)_s$ and $V_{J,s}$ are the s-th elements of $\mathbf{Ac}$ and $\mathbf{V}_J$, respectively. Then, by limiting the value of k to $k=0,1,..,K-1$, and by setting $s = rK + m$, with $r = 0, 1, .., |q| - 1$ and $m=0,1,..,K-1$, W_k in (22) can be developed as follows:

$$\begin{aligned} W_k = &\sum_{r=0}^{|q|-1}\sum_{m=0}^{K-1} \frac{A_m C_m}{|q|} \exp\Big(-\frac{2j\pi r}{q}(m \bmod |q|)\Big) \\ &\times \exp\Big(\frac{2j\pi k}{qK}(rK+m)\Big). \end{aligned} \tag{23}$$

Then, for any $k=0,1,..,K-1$, and $p=0,..,|q-1|$, we develop W_{k+pK} to obtain:

$$\begin{aligned} W_{k+pK} = &\sum_{r=0}^{|q|-1}\sum_{m=0}^{K-1} \frac{A_m C_m}{|q|} \exp\Big(-\frac{2j\pi r}{q}(m \bmod |q|)\Big) \\ &\times \exp\Big(\frac{2j\pi}{qK}(k+pK)(rK+m)\Big) \\ = &\sum_{r=0}^{|q|-1}\sum_{m=0}^{K-1} \frac{A_m C_m}{|q|} \exp\Big(-\frac{2j\pi r}{q}(m \bmod |q|)\Big) \\ &\times \exp\Big(\frac{2j\pi k}{qK}(rK+m)\Big) \exp\Big(\frac{2j\pi p}{q}(rK+m)\Big). \end{aligned} \tag{24}$$

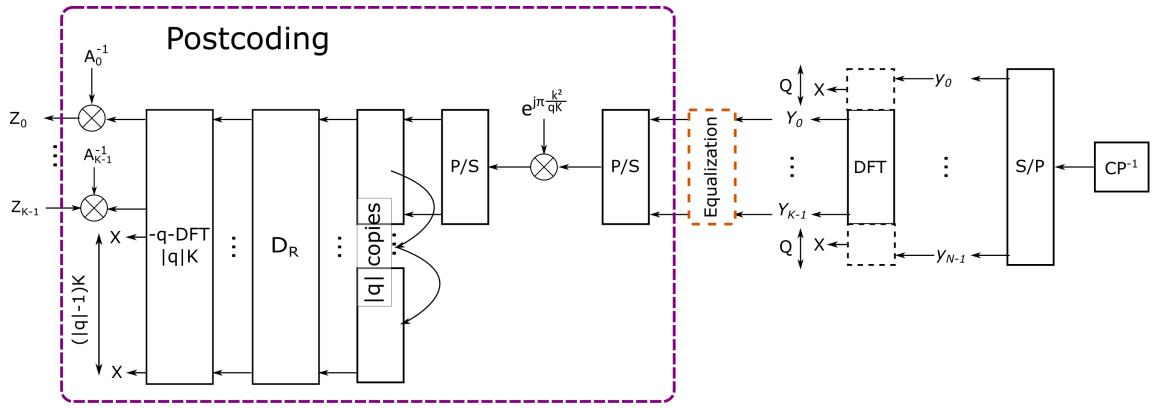

Fig. 5. DFT-based AFDM Demodulation.

Under the assumption that $\frac{K}{q} \in \mathbb{Z}$, we have $e^{\frac{2j\pi p}{q}(rK+m)} = e^{\frac{2j\pi pm}{q}}$, and since $e^{\frac{2j\pi pm}{q}} = e^{\frac{2j\pi m}{q}(p \bmod |q|)}$, hence W_{k+pK} in (24) simplifies to

$$W_{k+pK} = \sum_{r=0}^{|q|-1}\sum_{m=0}^{K-1} \frac{A_m C_m}{|q|} \exp\Big(-\frac{2j\pi(r-p)}{q}(m \bmod |q|)\Big) \times \exp\Big(\frac{2j\pi k}{qK}(rK+m)\Big). \quad (25)$$

We observe that W_{k+pK} in (25) is similar to W_k in (23) except that r is substituted by $(r-p)$ in the exponential, corresponding to a cyclic shift of the elements of $\mathbf{V}_J$ by pK positions. Hence, for any $k = 0,1,..,K-1$, and $p = 0,..,|q|-1$, we rewrite (25) by setting again $s = rK+m$, with $r = 0,1,..,|q|-1$ and $m = 0,1,..,K-1$, W_k, such as

$$W_{k+pK} = \sum_{s=0}^{|q|K-1} (Ac)_s V_{J,s}^{(p)} \exp\Big(\frac{2j\pi ks}{qK}\Big), \quad (26)$$

where $V_{J,s}^{(p)}$ are the elements of the $|q|K \times 1$ vector $\mathbf{V}_J^{(p)}$ defined by

$$\mathbf{V}_J^{(p)} = \mathbf{R}_p \mathbf{V}_J^T, \quad (27)$$

with $\mathbf{R}_p$ the $|q|K \times |q|K$ rotation matrix:

$$\mathbf{R}_p = \begin{pmatrix} \overbrace{0 \cdots 0}^{(|q|-p)K} & \overbrace{1\ 0 \cdots 0}^{pK} \\ \ddots & \ddots \\ & \ddots \quad 1 \\ 1 & \ddots \\ & \ddots \quad \ddots \\ 0 \cdots 0 & 1\ 0 \cdots 0 \end{pmatrix} \quad (28)$$

Finally, it should be noticed that the q-DFT of $\mathbf{R}_p$, defined as $\mathbf{D}_{R,p} = \boldsymbol{\mathcal{F}}_{|q|K}^{(q)} \mathbf{R}_p (\boldsymbol{\mathcal{F}}_{|q|K}^{(q)})^H$ is the $|q|K \times |q|K$ diagonal matrix that contains the elements $e^{2j\pi\frac{ip}{q}}$, $i = 0,1,..,|q|K-1$. Thus, for any $k = 0,1,..,K-1$, and $p = 0,..,|q|-1$, the element W_{k+pK} corresponds to the k-th element of the vector

$$\begin{aligned} \boldsymbol{\mathcal{F}}_{|q|K}^{(q)} \mathbf{D}_J^{(p)} \mathbf{Ac} &= \boldsymbol{\mathcal{F}}_{|q|K}^{(q)} \mathbf{R}_p \mathbf{D}_J \mathbf{Ac} \\ &= \boldsymbol{\mathcal{F}}_{|q|K}^{(q)} \mathbf{R}_p (\boldsymbol{\mathcal{F}}_{|q|K}^{(q)})^H \boldsymbol{\mathcal{F}}_{|q|K}^{(q)} \mathbf{D}_J \mathbf{Ac} \\ &= \mathbf{D}_{R,p} \mathbf{W} \\ \Leftrightarrow W_{k+pK} &= (\mathbf{D}_{R,p}\mathbf{W})(k) = e^{2j\pi\frac{kp}{q}} W_k, \end{aligned} \quad (29)$$

which concludes the proof. □

We deduce from Proposition 2 and (20) that the whole $|q|K$ elements of $\mathbf{W}$ can be defined by means of the K first samples of $\mathbf{W}$. Thus, even if the matrix $\mathbf{T}$ in (13) truncates the vector $\mathbf{W}$ (making the AFDM modulation operation in (13) and Fig. 3 *a priori* not bijective), it is possible to recover the vector $\mathbf{W}$ from $\mathbf{TW}$. In fact, from (29) we obtain that

$$\mathbf{W} = \mathbf{D}_R \mathbf{R}_{Id} \mathbf{TW}, \quad (30)$$

where $\mathbf{R}_{Id}$ is the $|q|K \times K$ matrix that vertically concatenates $|q|$ identity matrices $\mathbf{Id}_K$, namely

$$\mathbf{R}_{Id} = \overbrace{[1,..,1]}^{|q|}{}^T \otimes \mathbf{Id}_K,$$

which corresponds to $|q|-1$ copies of $\mathbf{TW}$, and $\mathbf{D}_R$ is the $|q|K \times |q|K$ diagonal matrix that contains the elements $e^{2j\pi\frac{kp}{q}}$ on its diagonal at indexes $(k+pK, k+pK)$ (in the case $\frac{N}{|q|}$ even), for any $k = 0,1,..,K-1$ and $p = 0,1,..,|q|-1$. This property can be applied at the receiver side as well to define an AFDM reception process such as described in Fig. 5, and mathematically formalized as follows.

We denote by y_n, $n = 0,1,..,N-1$, the samples of the received signal after CP removal and ignoring the effect of multipath channel. Then, $\mathbf{y}$ is the $N \times 1$ vector containing these samples, and we have $\mathbf{y} = \mathbf{x} + \mathbf{n}_o$ where the vector $\mathbf{n}_o$ contains the samples of the additive noise. Subsequently, by noticing that $\mathbf{x} = \boldsymbol{\mathcal{F}}_N^H \mathbf{O} \mathbf{D}_c \mathbf{TW}$, the demodulated data symbols Z_k, $k = 0,1,..,K-1$ within the $K \times 1$ vector $\mathbf{Z}$ can be expressed as

$$\mathbf{Z} = (\mathbf{A})^{-1} \mathbf{T} (\boldsymbol{\mathcal{F}}_{|q|K}^{(q)})^H \mathbf{D}_R \mathbf{R}_{Id} \mathbf{D}_c^H \bar{\mathbf{O}} \boldsymbol{\mathcal{F}}_N \mathbf{y}, \quad (31)$$

where $\bar{\mathbf{O}} = [\mathbf{0}_{K\times Q}, \mathbf{Id}_K, \mathbf{0}_{K\times Q}]$ is the $K \times N$ matrix corresponding to the null subcarriers removal. Note that in the case where $\frac{N}{|q|}$ is odd, (31) holds with $\mathbf{D}_R$ the $|q|K \times |q|K$ diagonal matrix that contains the elements $(-1)^p e^{2j\pi\frac{kp}{q}}$ on its diagonal at indexes $(k+pK, k+pK)$. Thus, in absence of noise,

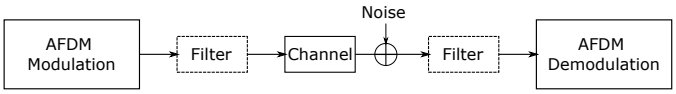

Fig. 6. AFDM modem setup composed of the suggested AFDM transmitter (13), a possible filtering stage [33], a channel (AWGN or multipath), the additive noise, and the AFDM receiver (see Section IV).

substituting $\mathbf{y}=\mathbf{x}$ into (31) straightforwardly leads to $\mathbf{Z}=\mathbf{C}$, where $\mathbf{C}=[C_0,C_1,..,C_{K-1}]^T$.

B. Input-Output Relation

In a more general case where the multipath channel is considered, the received signal $\mathbf{y}$ can be expressed as

$$\mathbf{y}=\sum_{l=0}^{L-1} h_l \mathbf{\Delta}_{\alpha_l} \mathbf{\Pi}^l \mathbf{x}+\mathbf{n}_o, \tag{32}$$

where h_l is the lth channel path coefficient, and L is the channel length. Moreover, $\mathbf{\Delta}_{\alpha_l}$ is the $N\times N$ diagonal matrix containing the samples $e^{2j\pi\frac{\alpha_l n}{N}}$, with α_l the normalized Doppler shift, and $\mathbf{\Pi}$ is the forward cyclic-shift matrix (see [9] for instance).

Subsequently, it is possible to equalize the received signal $\mathbf{y}$ in the frequency domain based on the suggested DFT-based AFDM receiver (instead of affine domain as usual, *e.g.* [29]), as illustrated in Fig. 5. Thus, (32) can be expressed in the frequency domain as

$$\begin{aligned}\mathbf{Y}&=\boldsymbol{\mathcal{F}}_N \sum_{l=0}^{L-1} h_l \mathbf{\Delta}_{\alpha_l} \mathbf{\Pi}^l \boldsymbol{\mathcal{F}}_N^H \boldsymbol{\mathcal{F}}_N \mathbf{x}+\boldsymbol{\mathcal{F}}_N \mathbf{n}_o \\ &=\mathbf{H}_{eq}\mathbf{X}+\mathbf{N}_o,\end{aligned} \tag{33}$$

where $\mathbf{H}_{eq}=\boldsymbol{\mathcal{F}}_N \sum_{l=0}^{L-1} h_l \mathbf{\Delta}_{\alpha_l} \mathbf{\Pi}^l \boldsymbol{\mathcal{F}}_N^H$ is the equivalent channel matrix gathers the contributions of the multipath coefficients and the Doppler spread in the frequency domain. Furthermore, from (13), the vector $\mathbf{X}$ has a closed-form expression given by $\mathbf{X}=\mathbf{O}\mathbf{D}_c\mathbf{T}\boldsymbol{\mathcal{F}}_{|q|K}^{(q)}\boldsymbol{\gamma}$. Considering the minimum mean square error (MMSE) equalization method, the signal $\mathbf{X}$ is recovered by applying

$$\hat{\mathbf{X}}=\mathbf{H}_{eq}^H\Big(\mathbf{H}_{eq}\mathbf{H}_{eq}^H+\mathbb{E}\{\mathbf{N}_o\mathbf{N}_o^H\}\Big)^{-1}\mathbf{Y}, \tag{34}$$

where $\mathbb{E}\{.\}$ is the mathematical expectation. Moreover, note that in practice, the channel matrix $\mathbf{H}_{eq}$ can be substituted by its estimate (see [29] for channel estimation in AFDM). Then, the equalized signal $\hat{\mathbf{X}}$ can be processed as in (31) and illustrated in Fig. 5.

V. Numerical Results

A. Simulations Setup and Parameters

In this section, we analyze the performance of the suggested AFDM modulation and demodulation methods according to three different typical sources of distortion: filtering, coloured noise, and time-frequency selective channel. The general simulations setup is illustrated in Fig. 6: the transmitter is based on the proposed solution, a possible filtering stage allowing to shape the AFDM spectrum and to limit the out-of-band emission (OOBE) [16], [33], a channel (flat or multipath), the additive noise (white or coloured), and the AFDM receiver suggested in Section IV. Eventually, a memoryless nonlinear power amplifier can be considered, if indicated. It is generated by means of the communications toolbox of matlab. Note that in practice, Solution (13) has been used, but simulations (not shown in this paper) show that other solutions (*e.g.*. (12) and (17)) are actually equivalent. Furthermore, the performance of the AFDM is compared with the OFDM and the OTFS waveforms. The latter is composed of block modulation of $M=8$ consecutive symbols. Each of them are shaped with a rectangular window, such that a simple DFT-based OTFS modulation such as [10] is performed (see Section II.A in [10]). Note that the number of considered subcarriers is the same for AFDM, OFDM, and OTFS.

To show the compliance of the AFDM waveform with 3GPP and such as considered in [16], we consider that $N=1024$ and $K=600$ in all simulations, and a subcarrier spacing of 30 kHz. It is worth noticing that under this condition, we can have $|q|=2,3,4,5,6$ and other larger values, which allows for a wide choice of the value q leading to $\frac{K}{q}\in\mathbb{N}$. The value of α is arbitrarily set to $\alpha=2$. Furthermore, a CP of length $N_{CP}=\frac{1}{8}N$ is considered, as well as a 64-QAM constellation for the data symbols C_k. To recover the symbols, a simple frequency domain MMSE equalizer is used at the reception side, assuming that the channel is known (or perfectly estimated). More elaborated channel estimation and equalization techniques can be found in [9], [27]–[30], but it is out of the scope of this paper. All the BER results have been obtained using Matlab, and averaged over at least 10^3 independent simulations runs.

B. Filtered-AFDM (f-AFDM)

We first analyze the positive and disruptive effects of a filter allowing to spectrally shape the AFDM signal. In fact, as many multicarrier waveform carried by a square window, the AFDM is prone to high OOBE. To reduce the latter in 5G (OFDM), a filtering method at both transmission and reception has been suggested in [33], and later applied to OCDM in [16]. Therefore, we consider the same filter, whose impulse response is given by:

$$f_n=\frac{p_n w_n}{\sum_n p_n w_n}, \tag{35}$$

where $-\lfloor\frac{L_F}{2}\rfloor\leq n\leq\lfloor\frac{L_F}{2}\rfloor$ and L_F is the length of the filter. Moreover, p_n and w_n are expressed as

$$p_n=\mathrm{sinc}\left(\frac{K+2\delta_w}{N}.n\right), \tag{36}$$

and

$$w_n=\left(0.5\Big(1+\cos\Big(\frac{2\pi n}{L_F-1}\Big)\Big)\right)^{0.6}, \tag{37}$$

respectively. The parameter δ_w^i in (36) is the so-called tone offset, which ensures that the resulting filter has a flat passband over the entire signal bandwidth. Such as indicated in Fig. 6, the filter is applied directly after the modulation, which is made possible by means of the proposed solutions leading to AFDM signal sampled at the desired rate.

Fig. 7 shows the power spectral density (PSD) of the filtered-AFDM (f-AFDM) signal ($q=-2$) versus the normalized frequency and considering $L_F=1$ (AFDM without filtering), 129, and 257. To show the effect of the eventually used power amplifier, the PSD of the f-AFDM signal with $L_F=257$ at the output of the amplifier is plotted as well. It can be observed that the OOBE of f-AFDM without amplification is drastically reduced (up to 100 dB) compared with AFDM. The same result is observed for OFDM [33] and OCDM [16]. However, the filter

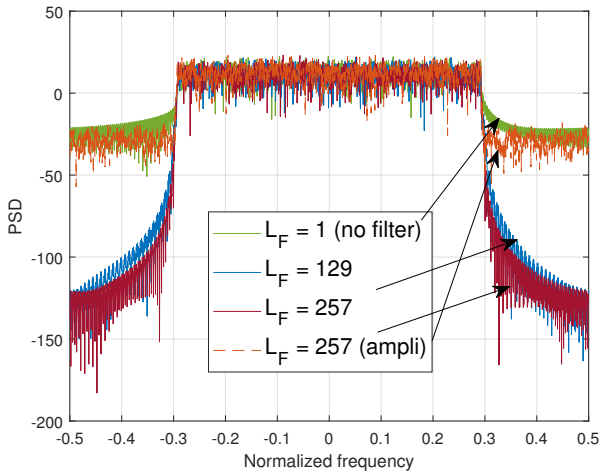

Fig. 7. PSD of f-AFDM versus normalized frequency for $L_F = 1$ (AFDM), 129, and 257.

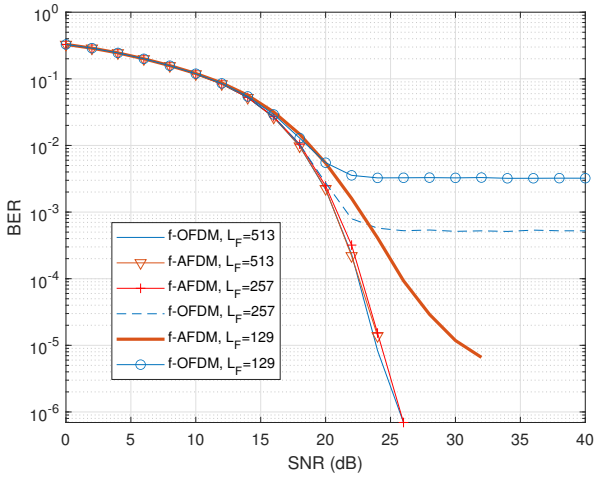

Fig. 8. BER versus SNR (dB) of f-AFDM compared with f-OFDM for $L_F = 129$, 257, and 513.

inevitably induces distortions, in particular at the edge of the passband despite the addition of the tone offset. Furthermore, the longer the filter, the higher the complexity, which can be limiting in practice. In addition, we observe that the use of the amplifier largely increases the OOBE due to the non-linearity, and since AFDM is prone to high PAPR. However, this could be attenuated thanks to usual pre-amplifiers used in OFDM systems to recover the good OOBE feature of f-AFDM.

To analyze the effect of these distortions, Fig. 8 shows the BER versus SNR (dB) of f-AFDM compared with filtered-OFDM (f-OFDM) [33] for $L_F = 129$, 257, and 513 in AWGN and considering a 64-QAM. It can be observed that f-AFDM with $L_F \in \{257,513\}$ and f-OFDM with $L_F = 513$ achieve the same BER performance. Otherwise, the performance of f-AFDM with $L_F = 129$ is slightly degraded, while the BER of f-OFDM with $L_F \in \{129,257\}$ reaches a lower bound of 5.10^{-4} and 3.10^{-3}, respectively, for SNR values larger than 25 dB. Thus, Figs. 7 and 8 show that the longer the filter, the lower the OOBE and the BER, but at the same time the higher the complexity. However, f-AFDM is more robust to the distortions induced by the filter than f-OFDM, and allows for an excellent trade-off between performance and complexity, *e.g.* f-AFDM $L_F = 257$ achieves the same BER performance as $L_F = 513$ and reduces the OOBE by 100 dB. This good feature comes from the capability of AFDM to spread the errors induced by the filter over all the subcarriers, whereas it is concentrated on the edge subcarriers in OFDM.

C. AFDM in Coloured Noise

In this second series of simulations, we analyze the effect of a coloured noise on the performance of the AFDM compared with OFDM and OTFS. To simulate the additive coloured noise, we arbitrarily filter the AWGN by the 4-tap filter $g = \frac{1}{2}[1,1,1,1]$, whose PSD (normalized by the maximum value) is given in Fig. 9 versus the subcarriers numbers. Note that any other model of noise could be considered as well. In practice, such a coloured noise could mimic the effect of the radio frequency (RF) chain (including analog to digital converter, downsampling, as well as other RF imperfections) or the presence of interferers within the band. Otherwise, the same simulations parameters as previously are considered.

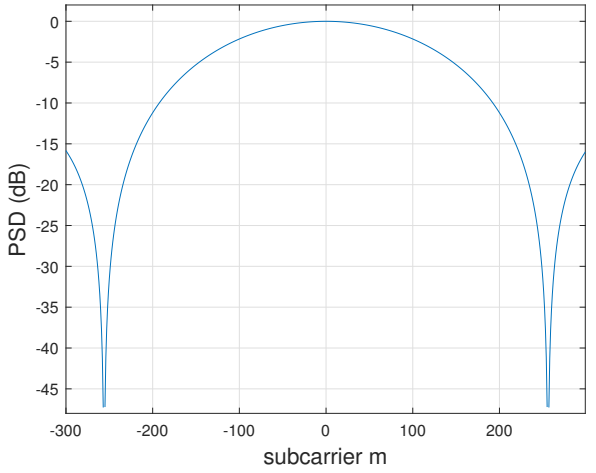

Fig. 9. PSD of the considered filtered noise versus the subcarrier indexes m.

Fig. 10 shows the BER performance versus SNR (dB) of AFDM compared with OFDM and OTFS. It can be observed that for low SNR range (typically SNR$\leq$10 dB), AFDM, OFDM, and OTFS achieve almost the same BER performance. For larger SNR values, AFDM and OTFS outperforms OFDM, with a gain of 2 dB at BER$= 10^{-4}$ for instance. We also observe that AFDM slightly outperforms OTFS in the SNR range >16 dB, but without significant gain (1 dB at BER$= 10^{-6}$). Such a behaviour of AFDM and OTFS in colored noise should be further investigated. However, this shows the inherent robustness of AFDM against coloured noise and interference, thanks to the property of AFDM to spread the errors over all subcarriers.

D. AFDM in Time Frequency Selective Channel

Other series of simulations analyze the performance of the AFDM signal in a time and frequency selective channel. To this end, we considered the tapped delay line (TDL)-C channel defined by 3GPP in Section 7.7 of [34]. It is a 24-taps channel with a maximum delay spread of 8.65 ns. The same parameters as previous are used, and we also define the carrier frequency f_c

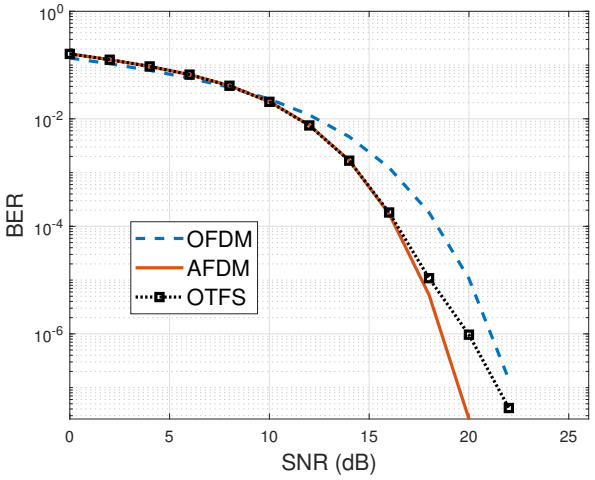

Fig. 10. BER versus SNR (dB) of AFDM compared with OFDM and OTFS in coloured noise.

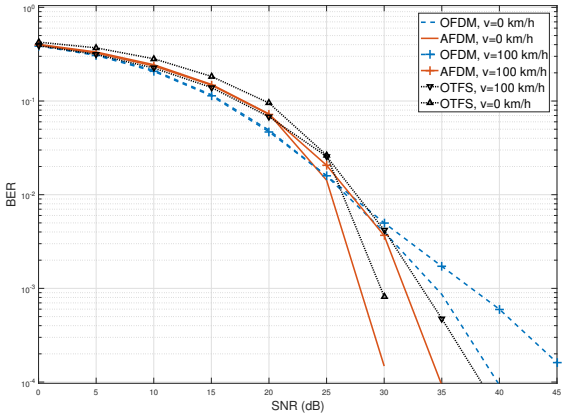

Fig. 11. BER versus SNR (dB) of AFDM compared with OFDM and OTFS in TDL-C channel.

such that $f_c = 2$ GHz. Fig. 11 compares the BER versus SNR of AFDM and OFDM for two scenarios of mobility $v = 0$ km/h (static) and $v = 100$ km/h (namely a Doppler spread θ_D of about 185 Hz). It can be observed that in both cases, both AFDM and OTFS outperform OFDM for SNR>25 dB. These results shows the capability of AFDM to be more robust against time-frequency selective channels than OFDM, which are corroborated by those in [9], [27]. Moreover, it can be observed that AFDM slightly outperforms OTFS by 1 dB at BER = 10^{-3}. This may be due to the use of the frequency domain MMSE equalizer for both AFDM and OTFS modulation schemes. It emphasizes that AFDM is more adapted to frequency domain equalization than OTFS because it is a per-symbol modulation whereas OTFS is a block modulation. More dedicated equalizers must be considered for OTFS [35], [36], that are performed after the block demodulation to achieve full-diversity, but this is out of the scope of the paper.

E. BLER Performance

To compare the overall performance of AFDM with OFDM and OTFS, Fig. 12 shows the block error rate (BLER) versus SNR (dB) of the three modulations, considering the non-linear

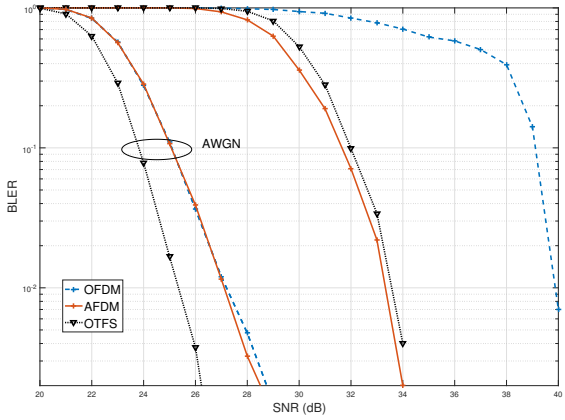

Fig. 12. BLER versus SNR (dB) of turbo-coded AFDM compared with OFDM and OTFS in AWGN TDL-C channel, and considering a power amplifier.

amplifier and a turbo-code with a rate 1/3. The input bits are randomly interleaved, and the turbo-decoder performs four iterations. The granularity of the block used to assess the BLER performance is the AFDM/OFDM symbol. The other parameters are the same as those used to obtain Fig. 11, with $v = 100$ km/h. Furthermore, the BLER performance of the three waveforms in AWGN (but with power amplifier) has been plotted as well for reference.

It can be observed that the BLER trajectories of AFDM and OFDM in AWGN match, whereas OTFS outperforms AFDM and OFDM. This shows that: i) AFDM and OFDM are more sensitive to the non linearity of the power amplifier than OTFS, because the PAPR of OTFS is lower than that of AFDM and OFDM, and ii) AFDM and OFDM achieve the same performance in the presence of AWGN and a non-linear power amplifier. In the case of multipath channel and mobility, we can observe that the BLER trajectories of AFDM and OTFS almost match. Compared with Fig. 11, this shows once again that AFDM is more sensitive to the non-linearity of the amplifier than OTFS. Moreover, Fig. 12 shows that AFDM outperforms OFDM by 6 dB at BLER=0.01. This confirms that the AFDM is much more robust against the disruptive combined effects of the channel, the mobility, and the non-linearity of the amplifier than OFDM. Such a large performance gap may be explained by the fact that the turbo-coded AFDM whitens the induced errors twice: inherently through the modulation and by using the interleaving, whereas the interleaving alone is not enough to achieve such a performance in turbo-coded OFDM.

VI. Conclusion

In this paper, we introduce DFT-based modulation and demodulation techniques for the AFDM waveform. Consequently, AFDM can be regarded as a simple precoded OFDM modulation, ensuring easy backward compatibility with OFDM-based technologies and standards. Additionally, the suggested approach allows signal generation at any desired sampling rate. To achieve this advantageous feature, two necessary conditions are established for the affine parameter q and the number of subcarriers N. Specifically, it is demonstrated that q or N must be even integers, and the ratio $\frac{N}{q}$ must be integer as well. Based on these conditions, a generic modulations and demodulation

scheme is developed, supported by theoretical analyses and proofs. It is proved to be less complex than a benchmark solution which involves the typical AFDM modulation followed by a DFT/IDFT upsampling stage. Numerical results show that AFDM consistently outperforms OFDM, displaying inherent robustness against various sources of distortion. This aligns with existing literature on AFDM. Furthermore, the performance of AFDM is shown to be comparable to that of OTFS. This paper lays the groundwork for further studies, including the adaptation of DFT-based AFDM (de)modulation methods to MIMO, the exploration of frequency precoding, channel estimation, and equalization, and the definition of multi-numerology AFDM signals. Furthermore, complementary performance results should also include different channel coding methods in future works.

APPENDIX

Proof of (9): By setting $k=r+|q|p$, with $p=0,1,..,\frac{N}{|q|}-1$, and $r=m \mod |q|$, we can develop:

$$\begin{aligned}
&\frac{1}{\sqrt{N}}\sum_{k=0}^{N-1}\Phi_{m,k}e^{2j\pi\frac{kn}{N}}= \\
&\frac{A_m}{\sqrt{N}}\sum_{k=0}^{N-1}\mathbb{1}_{(m-k)\mathrm{mod}\ q=0}\exp\Big(\frac{j\pi}{qN}(-k^2+2mk)\Big)e^{2j\pi\frac{kn}{N}} \\
=&\frac{A_m}{\sqrt{N}}\sum_{p=0}^{\frac{N}{|q|}-1}\exp\Big(\frac{j\pi}{qN}(-(r+|q|p)^2+2m(r+|q|p))\Big) \\
&\times\exp\Big(2j\pi\frac{(r+|q|p)n}{N}\Big) \\
=&\frac{A_m}{\sqrt{N}}\exp\Big(\frac{-j\pi r^2}{qN}+\frac{2j\pi rm}{qN}+\frac{2j\pi rn}{N}\Big) \\
&\times\sum_{p=0}^{\frac{N}{|q|}-1}\exp\Big(\frac{j\pi|q|}{N}\Big(-\varepsilon_q p^2-\frac{2rp}{q}+\frac{2mp}{q}+2np\Big)\Big). \qquad (38)
\end{aligned}$$

We use the development of the generalized Gaussian sum to simplify (38) as

$$\begin{aligned}
&\frac{1}{\sqrt{N}}\sum_{k=0}^{N-1}\Phi_{m,k}e^{2j\pi\frac{kn}{N}}= \\
&\frac{A_m}{\sqrt{N}}\exp\Big(\frac{-j\pi r^2}{qN}+\frac{2j\pi rm}{qN}+\frac{2j\pi rn}{N}\Big) \\
&\times\sqrt{\frac{N}{|q|}}\exp\Big(\frac{-j\pi|q|}{4\varepsilon_q N}\big(\frac{N}{|q|}-(-\frac{2r}{q}+\frac{2m}{q}+2n)^2\big)\Big) \\
&\times\underbrace{\sum_{p=0}^{|\varepsilon_q|-1}\exp\Big(\frac{j\pi}{\varepsilon_q}\Big(\frac{N}{|q|}p^2+(-\frac{2r}{q}+\frac{2m}{q}+2n)p\Big)\Big)}_{=1}, \qquad (39)
\end{aligned}$$

where the equality in the last line holds since $\frac{N}{q}$ is assumed to be even. After some mathematical simplifications, (39) reduces to

$$\begin{aligned}
\frac{1}{\sqrt{N}}\sum_{k=0}^{N-1}\Phi_{m,k}e^{2j\pi\frac{kn}{N}}=&\exp\Big(\frac{j\pi}{N}(qn^2+\alpha m^2+2mn)\Big) \\
=&\phi_{m,n}, \qquad (40)
\end{aligned}$$

which concludes the proof.

REFERENCES

[1] H. Tataria, M. Shafi, M. Dohler, and S. Sun, "Six critical challenges for 6g wireless systems: A summary and some solutions," *IEEE Vehicular Technology Magazine*, vol. 17, no. 1, pp. 16–26, March 2022.

[2] M. Chafii, L. Bariah, S. Muhaidat, and M. Debbah, "Twelve Scientific Challenges for 6G: Rethinking the Foundations of Communications Theory," *IEEE Communications Surveys & Tutorials*, vol. 25, no. 2, pp. 868–904, Secondquarter 2023.

[3] H. Wymeersch, A. Pärssinen, T. E. Abrudan, A. Wolfgang, K. Haneda, M. Sarajlic, M. E. Leinonen, M. F. Keskin, H. Chen, S. Lindberg, P. Kyösti, T. Svensson, and X. Yang, "6G Radio Requirements to Support Integrated Communication, Localization, and Sensing," in *2022 Joint European Conference on Networks and Communications & 6G Summit (EuCNC/6G Summit)*, June 2022, pp. 463–469.

[4] Q. Wang, A. Kakkavas, X. Gong, and R. A. Stirling-Gallacher, "Towards Integrated Sensing and Communications for 6G," in *2022 2nd IEEE International Symposium on Joint Communications & Sensing (JC&S)*, March 2022, pp. 1–6.

[5] A. Elzanaty, A. Guerra, F. Guidi, D. Dardari, and M.-S. Alouini, "Towards 6g holographic localization: Enabling technologies and perspectives," *IEEE Internet of Things Magazine*, pp. 1–7, April 2023.

[6] R. Hadani, S. Rakib, M. Tsatsanis, A. Monk, A. J. Goldsmith, A. F. Molisch, and R. Calderbank, "Orthogonal Time Frequency Space Modulation," in *2017 IEEE Wireless Communications and Networking Conference (WCNC)*, March 2017, pp. 1–6.

[7] F. Berggren and B. M. Popović, "Joint radar and communications with multicarrier chirp-based waveform," *IEEE Open Journal of the Communications Society*, vol. 3, pp. 1702–1718, September 2022.

[8] X. Ouyang and J. Zhao, "Orthogonal Chirp Division Multiplexing," *IEEE Transactions on Communications*, vol. 64, no. 9, pp. 3946–3957, 2016.

[9] A. Bemani, N. Ksairi, and M. Kountouris, "AFDM: A Full Diversity Next Generation Waveform for High Mobility Communications," in *2021 IEEE International Conference on Communications Workshops (ICC Workshops)*, 2021, pp. 1–6.

[10] W. Shen, L. Dai, J. An, P. Fan, and R. W. Heath, "Channel estimation for orthogonal time frequency space (otfs) massive mimo," *IEEE Transactions on Signal Processing*, vol. 67, no. 16, pp. 4204–4217, August 2019.

[11] L. Gaudio, M. Kobayashi, G. Caire, and G. Colavolpe, "On the effectiveness of otfs for joint radar parameter estimation and communication," *IEEE Transactions on Wireless Communications*, vol. 19, no. 9, pp. 5951–5965, September 2020.

[12] R. Bomfin, D. Zhang, M. Matthé, and G. Fettweis, "A Theoretical Framework for Optimizing Multicarrier Systems Under Time and/or Frequency-Selective Channels," *IEEE Communications Letters*, vol. 22, no. 11, pp. 2394–2397, 2018.

[13] R. Bomfin, M. Chafii, and G. Fettweis, "Low-Complexity Iterative Receiver for Orthogonal Chirp Division Multiplexing," in *2019 IEEE Wireless Communications and Networking Conference Workshop (WCNCW)*, 2019, pp. 1–6.

[14] L. G. d. Oliveira, M. B. Alabd, B. Nuss, and T. Zwick, "An OCDM Radar-Communication System," in *2020 14th European Conference on Antennas and Propagation (EuCAP)*, March 2020, pp. 1–5.

[15] L. G. de Oliveira, B. Nuss, M. B. Alabd, Y. Li, L. Yu, and T. Zwick, "Mimo-ocdm-based joint radar sensing and communication," in *2021 15th European Conference on Antennas and Propagation (EuCAP)*, March 2021, pp. 1–5.

[16] M. S. Omar and X. Ma, "Spectrum Design for Orthogonal Chirp Division Multiplexing Transmissions," *IEEE Wireless Communications Letters*, vol. 9, no. 11, pp. 1990–1994, 2020.

[17] V. Savaux, "Flexible communication system for 6g based on orthogonal chirp division multiplexing," in *2022 1st International Conference on 6G Networking (6GNet)*, July 2022, pp. 1–5.

[18] S.-C. Pei and J.-J. Ding, "Closed-form discrete fractional and affine Fourier transforms," *IEEE Transactions on Signal Processing*, vol. 48, no. 5, pp. 1338–1353, May 2000.

[19] M. Martone, "A multicarrier system based on the fractional Fourier transform for time-frequency-selective channels," *IEEE Transactions on Communications*, vol. 49, no. 6, pp. 1011–1020, June 2001.

[20] T. Erseghe, N. Laurenti, and V. Cellini, "A multicarrier architecture based upon the affine Fourier transform," *IEEE Transactions on Communications*, vol. 53, no. 5, pp. 853–862, May 2005.

[21] D. Stojanovic, I. Djurovic, and B. R. Vojcic, "Interference analysis of multicarrier systems based on affine Fourier transform," *IEEE Transactions on Wireless Communications*, vol. 8, no. 6, pp. 2877–2880, June 2009.

[22] ——, "Multicarrier communications based on the affine fourier transformin doubly-dispersive channels," *EURASIP Journal onWireless Communications and Networking*, vol. 2010, pp. 1 – 10, December 2010.

[23] A. Bemani, N. Ksairi, and M. Kountouris, "Affine Frequency Division Multiplexing for Next Generation Wireless Communications," *IEEE Transactions on Wireless Communications*, vol. 22, no. 11, pp. 8214–8229, November 2023.

[24] Y. Ni, Z. Wang, P. Yuan, and Q. Huang, "An AFDM-Based Integrated Sensing and Communications," 2022.
[25] A. Bemani, N. Ksairi, and M. Kountouris, "Integrated Sensing and Communications With Affine Frequency Division Multiplexing," *IEEE Wireless Communications Letters*, vol. 13, no. 5, pp. 1255–1259, May 2024.
[26] H. Yin, X. Wei, Y. Tang, and K. Yang, "Design and Performance Analysis of AFDM with Multiple Antennas in Doubly Selective Channels," 2022.
[27] A. Bemani, G. Cuozzo, N. Ksairi, and M. Kountouris, "Affine Frequency Division Multiplexing for Next-Generation Wireless Networks," in *2021 17th International Symposium on Wireless Communication Systems (ISWCS)*, 2021, pp. 1–6.
[28] A. Bemani, N. Ksairi, and M. Kountouris, "Low Complexity Equalization for Afdm In Doubly Dispersive Channels," in *ICASSP 2022 - 2022 IEEE International Conference on Acoustics, Speech and Signal Processing (ICASSP)*, May 2022, pp. 5273–5277.
[29] H. Yin and Y. Tang, "Pilot Aided Channel Estimation for AFDM in Doubly Dispersive Channels," in *2022 IEEE/CIC International Conference on Communications in China (ICCC)*, August 2022, pp. 308–313.
[30] W. Benzine, A. Bemani, N. Ksairi, and D. Slock, "Affine Frequency Division Multiplexing For Communications on Sparse Time-Varying Channels," *ArXiv*, pp. 1 – 6, June 2023.
[31] B. C. Berndt, R. J. Evans, and K. S. Williams, *Gauss and Jacobi Sums*. Ney York: John Wiley and Sons, 1996, ch. 1: Gauss Sums, pp. 7 – 56.
[32] H. Hassanieh, P. Indyk, D. Katabi, and E. Price, "Nearly optimal sparse fourier transform," in *STOC '12: Proceedings of the forty-fourth annual ACM symposium on Theory of computing*, May 2012, pp. 563 – 578.
[33] H. Huawei, "f-OFDM scheme and filter design, R1-165425," 3GPP, Tech. Rep., 2016.
[34] 3GPP, "Study on channel model for frequency spectrum above 6 GHz," 3GPP, Tech. Rep., July 2017.
[35] G. D. Surabhi and A. Chockalingam, "Low-Complexity Linear Equalization for OTFS Modulation," *IEEE Communications Letters*, vol. 24, no. 2, pp. 330–334, February 2020.
[36] J. Cheng, H. Gao, W. Xu, Z. Bie, and Y. Lu, "Low-Complexity Linear Equalizers for OTFS Exploiting Two-Dimensional Fast Fourier Transform," 2019.